RSC Advances

PAPER

View Article Online
View Journal | View Issue

Check for updates

Cite this: *RSC Adv.*, 2021, **11**, 23437

On-surface synthesis of π-conjugated ladder-type polymers comprising nonbenzenoid moieties†

José I. Urgel, ‡*[a] Julian Bock, [bc] Marco Di Giovannantonio, §[a] Pascal Ruffieux, [a] Carlo A. Pignedoli,[a] Milan Kivala *[bc] and Roman Fasel *[ad]

Received 26th April 2021
Accepted 1st June 2021

DOI: 10.1039/d1ra03253d

rsc.li/rsc-advances

On-surface synthesis provides a powerful approach toward the atomically precise fabrication of π-conjugated ladder polymers (CLPs). We report herein the surface-assisted synthesis of nonbenzenoid CLPs from cyclopenta-annulated anthracene monomers on Au(111) under ultrahigh vacuum conditions. Successive thermal annealing steps reveal the dehalogenative homocoupling to yield an intermediate 1D polymer and the subsequent cyclodehydrogenation to form the fully conjugated ladder polymer. Notably, neighbouring monomers may fuse in two different ways, resulting in six- and five-membered rings, respectively. The structure and electronic properties of the reaction products have been investigated *via* low-temperature scanning tunneling microscopy and spectroscopy, complemented by density-functional theory calculations. Our results provide perspectives for the on-surface synthesis of nonbenzenoid CLPs with the potential to be used for organic electronic devices.

Open Access Article. Published on 02 July 2021. Downloaded on 2/7/2026 7:14:46 PM.
This article is licensed under a Creative Commons Attribution-NonCommercial 3.0 Unported Licence.

Conjugated ladder polymers (CLPs) represent an attractive type of π-conjugated polymers which consist of a sequence of fused rings with adjacent rings sharing two or more atoms.[1] The restriction of bond rotations inherent to CLPs represent an important approach that has been systematically pursued since the 1990s.[2,3] Such rigidification generally provides enhanced intermolecular π–π stacking interactions and high thermal stability, which may lead to application-relevant properties (or improved materials properties),[4–10] with prospects in organic field-effect transistors,[11] organic light emitting diodes,[12] gas separation[13,14] or optically pumped lasers.[15] While the majority of CLPs reported to date have been obtained through solution chemistry,[16,17] the potential of on-surface synthesis to overcome some of the intrinsic challenges of solution-based approaches, including low solubility, high reactivity of reaction products or precursors and limited diversity of reaction designs, toward the effective fabrication of tailored ladder polymers[18–20] has increasingly come to forth in the last decade only.[21]

In this context, graphene nanoribbons (GNRs)[22] represent the most acknowledged class of CLPs. Despite the recent expansion of the GNR catalogue, the controlled incorporation of nonbenzenoid rings into the GNR backbone to modulate the structural[23,24] and electronic[25,26] properties remains comparably scarce. Theoretical calculations have anticipated the existence of several nonbenzenoid carbon allotropes which are expected to exhibit pronouncedly different (opto)-electronic properties,[27,28] mechanical stability,[29,30] or electron transport properties.[31] Only recently, the on-surface synthesis of several CLPs containing nonbenzenoid rings has been reported.[32–38] Nevertheless, systematic investigations of the structural and electronic properties resulting from selective incorporation of nonbenzenoid rings into CLPs are still lacking.

In this work, we introduce an exemplary approach toward the on-surface formation of nonbenzenoid π-conjugated ladder-type polymers on a coinage metal surface under ultra-high vacuum (UHV) conditions. To this end, we synthesized in solution 2,7-dibromocyclopenta[*hi*]aceanthrylene as a precursor (**1**),[39] which features electron acceptor properties due to the presence of the 5-membered rings.[39,40] Compound **1** can be sublimed intactly and converted to nonbenzenoid CLPs (**3**) by thermal activation on the metal surface (see ESI† for the precursor synthesis and characterization). The reaction route toward the formation of the CLP **3**, illustrated in Scheme 1, follows two surface-assisted steps including dehalogenative homocoupling to yield an intermediate one-dimensional (1D) polymer (**2**) and cyclodehydrogenation to form **3**. Interestingly, two different carbon–carbon (C–C) bonds between adjacent

[a]*Empa, Swiss Federal Laboratories for Materials Science and Technology, 8600 Dübendorf, Switzerland. E-mail: jose-ignacio.urgel@imdea.org; roman.fasel@empa.ch*

[b]*Institute of Organic Chemistry, Ruprecht-Karls-University Heidelberg, Im Neuenheimer Feld 270, 69120 Heidelberg, Germany. E-mail: milan.kivala@oci.uni-heidelberg.de*

[c]*Centre for Advanced Materials, Ruprecht-Karls-University Heidelberg, Im Neuenheimer Feld 225, 69120 Heidelberg, Germany*

[d]*Department of Chemistry and Biochemistry, University of Bern, 3012 Bern, Switzerland*

† Electronic supplementary information (ESI) available. See DOI: 10.1039/d1ra03253d

‡ Present address: IMDEA Nanoscience, C/ Faraday 9, Campus de Cantoblanco, 28049 Madrid, Spain.

§ Present address: Istituto di Struttura della Materia-CNR (ISM-CNR), via Fosso del Cavaliere 100, 00133 Roma, Italy.

© 2021 The Author(s). Published by the Royal Society of Chemistry

Open Access Article. Published on 02 July 2021. Downloaded on 2/7/2026 7:14:46 PM.
This article is licensed under a Creative Commons Attribution-NonCommercial 3.0 Unported Licence.

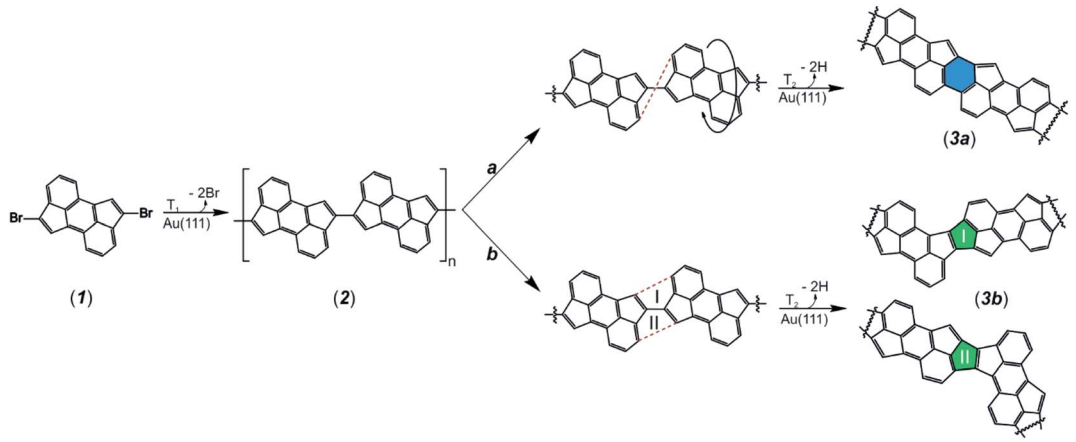

Scheme 1 On-surface synthesis of nonbenzenoid CLPs **3a** and **3b**.

monomers can be formed in the cyclodehydrogenation step, resulting in six- or five-membered ring formation between monomers (**3a** and **3b**, respectively). All the synthesis steps are investigated by scanning tunneling microscopy (STM) and complemented by density-functional theory (DFT).

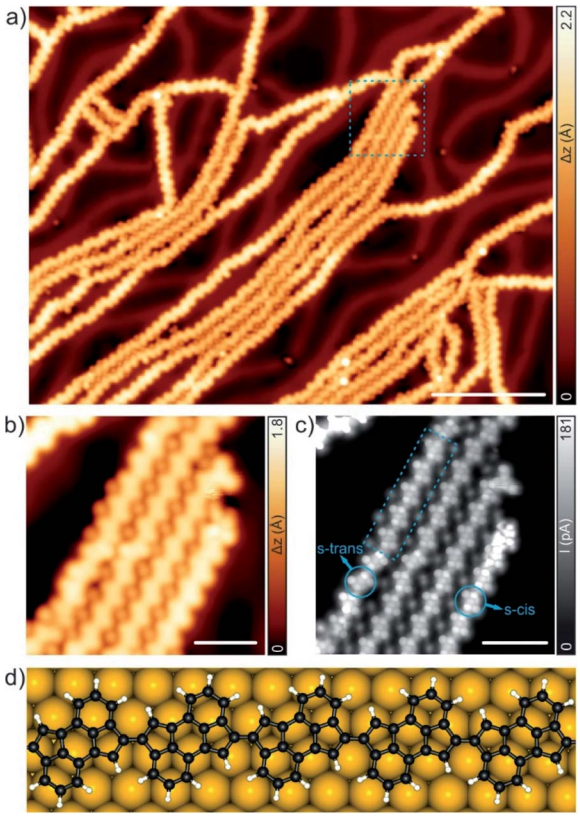

Fig. 1 On-surface synthesis of the 1D polymer (**2**) on Au(111). (a) Overview STM topography image of the surface after deposition of **1** and subsequent annealing at 330 °C, showing the predominant presence of 1D chains. $V_b = -0.50$ V, $I_t = 60$ pA, scale bar: 10 nm. (b) High-resolution STM image of (a) where 1D chains together with rounded protrusions, assigned to bromine atoms, are observed. $V_b = -0.20$ V, $I_t = 70$ pA, scale bar: 2 nm. (c) CO-functionalized UHR-STM image of **2** where the intramolecular features of the nonbenzenoid molecular backbone in the polymers are discerned. *S-cis* and *s-trans* denote the two isomers found within a chain. $V_b = 5$ mV, $I_t = 70$ pA, scale bar: 2 nm. (d) Top view of the DFT equilibrium geometry of **2** on Au(111).

The chemical structure of **2** and **3** are unambiguously identified by ultrahigh-resolution STM (UHR-STM) and their electronic properties studied by scanning tunneling spectroscopy (STS).

To study the on-surface reactions illustrated in Scheme 1, we sublimed precursor **1** onto an atomically clean Au(111) surface held at room temperature and subsequently annealed at 330 °C. High-resolution STM images (Fig. 1a and b) reveal the predominant presence of 1D polymers together with rounded protrusions between the chains, which we assign to bromine atoms detached from **1**. To confirm the chemical structure of **2**, ultrahigh-resolution STM (UHR-STM) images acquired with a CO-functionalized tip recorded in the Pauli repulsion regime[41,42] were performed (Fig. 1c). Hereby, intramolecular features corresponding to the cyclopenta[*hi*]aceanthrylene molecular backbone linked *via* C–C bonds through the pentagons of each molecular subunit are distinguished (see Fig. S1† for a detailed STS and voltage dependent differential conductance spectra characterization of a segment of **2**). Additionally, UHR-STM images allow us to discern single (*s*)-*trans* and -*cis* isomers within the same polymer chain (see Scheme S1† for the reaction pathway between adjacent *s-trans* and *s-cis* isomers). The DFT-optimized equilibrium geometry of **2** shown in Fig. 1d indicates that the polymer adopts a planar configuration, with an adsorption height of 3.3 Å with respect to the underlying gold surface.

Annealing the sample at 400 °C induced minor variations in the molecular structure of **2** and only small segments of the 1D polymer (~8%), attributed to the onset of the cyclodehydrogenation reaction, present a different appearance (see Fig. S2† for STM and UHR-STM images). Only after a further annealing step at 420 °C, the formation of the targeted CLP **3**, coexisting with a few laterally fused segments, is achieved (Fig. 2a). A zoom-in STM image (Fig. 2b), allows us to discern two different C–C coupling motifs in the formation of **3**. Herein, the kinked/linear segments observed in Fig. 2b are attributed to the formation of a hexagon/pentagon (**3a**/**3b**) between two molecular units (Fig. 2c and d). Importantly, statistics over the

© 2021 The Author(s). Published by the Royal Society of Chemistry

Open Access Article. Published on 02 July 2021. Downloaded on 2/7/2026 7:14:46 PM.
This article is licensed under a Creative Commons Attribution-NonCommercial 3.0 Unported Licence.

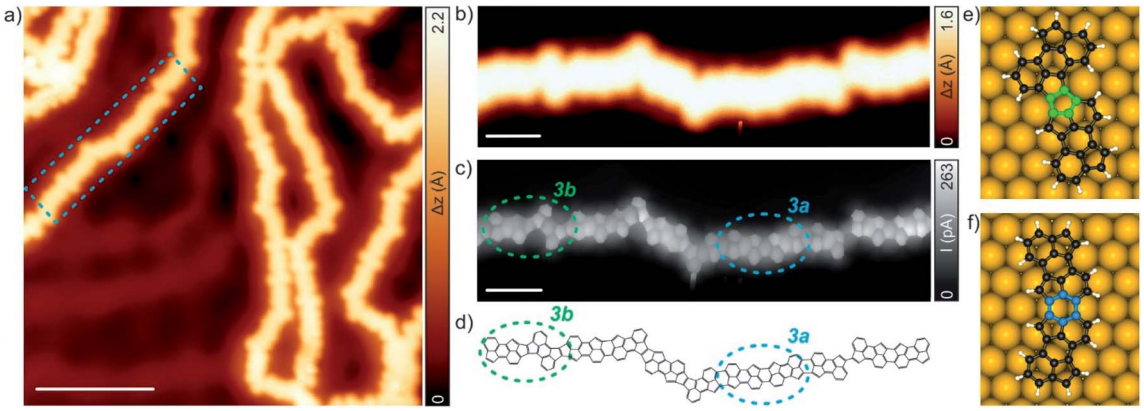

Fig. 2 On-surface synthesis of **3** on Au(111). (a) Overview STM topography image of the surface after annealing **2** at 420 °C, showing the formation of fully conjugated nonbenzenoid CLPs. $V_b = -0.10$ V, $I_t = 100$ pA, scale bar: 5 nm. (b) High-resolution STM image of **3** where kinked and linear segments can be distinguished. $V_b = 0.02$ V, $I_t = 100$ pA, scale bar: 1 nm. (c and d) CO-functionalized UHR-STM image and corresponding chemical sketch of the segment of **3** shown in (b) where the intramolecular features, attributed to the formation of a six-membered (**3a**) and a five-membered (**3b**) ring, respectively, are discerned. $V_b = 5$ mV, $I_t = 100$ pA, scale bar: 1 nm. (e and f) Top views of the DFT equilibrium geometry of **3b** and **3a** respectively, on Au(111). Bonds and atoms highlighted in green and blue colours show the pentagon and hexagon formed due to the cyclodehydrogenation reaction.

coupling motifs observed for more than 500 molecular units indicates that the coupling through the six-membered ring is favoured over the five-membered one (**3a** = 58%, **3b** = 32%, non-cyclodehydrogenated = 10%). This can be rationalized on the basis of simple energetic considerations. On the one hand, gas phase calculations for **3a** and **3b** reveal that **3a** is ≈1 eV more energetically favoured compared to **3b**. This energy difference is further enhanced on the substrate and **3a** (Fig. 2f) is ≈1.7 eV more stable compared to **3b** on Au(111). Configurations of the polymer units that would lead to the formation of **3b** motifs are hindered by the fact that the polymer should undergo a torsion (deviating from linearity) that is unlikely to occur for long strands. Therefore, cyclodehydrogenation between adjacent *s-trans*/*s-cis* and *s-cis*/*s-trans* isomers (synthetic pathway (a) in Scheme S1†) implies the formation of a new hexagon (**3a**), while cyclodehydrogenation between adjacent *s-trans*/*s-trans* and *s-cis*/*s-cis* isomers (synthetic pathway (b) in Scheme 1) affords the formation of a new pentagon (**3b**, with **3bI**, **3bII** ≈ 50%). In addition, it is expected that the reaction mechanisms in the formation of **3a** and **3b** involve a rotation of cyclopenta[*hi*]aceanthrylene molecular units on the surface substrate, at temperatures typical for the annealing, prior to cyclization (see synthetic pathway (a) in Scheme 1 and synthetic pathway (b) in Scheme S1†).[32,43,44] Finally, Fig. 2e and f display the DFT equilibrium geometry of the formed pentagon (in green in Fig. 2e) and hexagon (in blue in Fig. 2f), respectively. Both adopt a planar configuration, with an adsorption height of 3.2 Å with respect to the underlying surface.

Next, we performed STS measurements on a **3a** segment (six consecutive units), whose formation is favoured over **3b**, to probe its electronic structure. Voltage-dependent differential conductance spectra (d*I*/d*V vs. V*) feature characteristic peaks at −1.12 eV and +0.65 eV (Fig. 3a), which are assigned to the valence band minimum (VBM) and the conduction band maximum (CBM), respectively, corresponding to an electronic

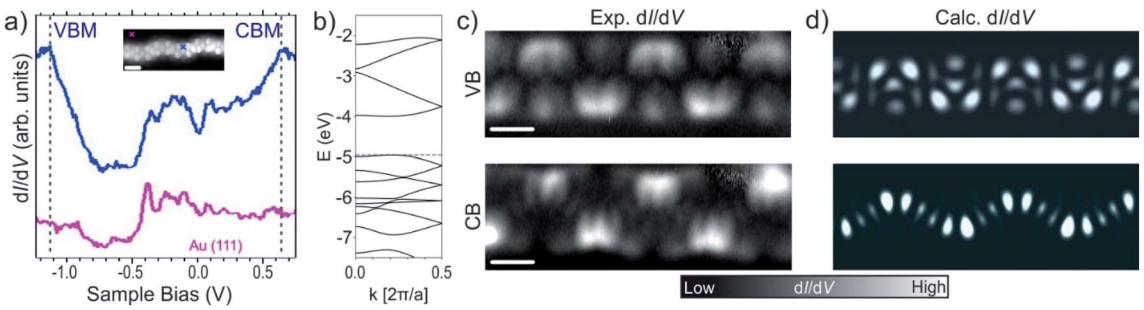

Fig. 3 Electronic properties of **3a** on Au(111). (a) d*I*/d*V* spectrum of **3a**, acquired at the position indicated by the blue cross (blue line), revealing a band gap of 1.77 eV, and reference spectrum taken on the bare Au(111) surface (pink line). (b) DFT calculated band structure of an infinite CLP **3a** in gas phase. (c and d) Constant-current differential conductance (d*I*/d*V*) maps (c) and corresponding DFT-calculated LDOS maps (d) at the energetic positions corresponding to the VB (top) and the CB (bottom) of **3a**, respectively. Tunneling parameters for the d*I*/d*V* maps: VB ($V_b = -1.10$ V, $I_t = 300$ pA); CB ($V_b = 0.70$ V, $I_t = 300$ pA). All scale bars: 0.5 nm.

© 2021 The Author(s). Published by the Royal Society of Chemistry

Open Access Article. Published on 02 July 2021. Downloaded on 2/7/2026 7:14:46 PM.
This article is licensed under a Creative Commons Attribution-NonCommercial 3.0 Unported Licence.

bandgap of 1.77 eV on Au(111), matching very well with the calculated band structure for an infinite **3a** segment (Fig. 3b). Constant-current maps of the dI/dV signal of a **3a** acquired with a CO-functionalized tip at the VBM (top) and CBM (bottom) energetic positions are shown in Fig. 3c (see Fig. S3 and S4† for comparison with the constant-height dI/dV maps of **3a** as well as dI/dV *vs.* V and constant-current dI/dV maps of the minority **3b** segment, respectively). Finally, the experimental dI/dV maps are well reproduced by the DFT-calculated local density of states (LDOS) maps for the CBM and VBM (Fig. 3d), calculated at 3 Å above the molecular plane.

In conclusion, we have demonstrated a novel synthetic pathway toward the on-surface fabrication of nonbenzenoid π-conjugated ladder-type polymers on Au(111) by a combination of high-resolution STM and STS complemented with DFT calculations. A first annealing step at 330 °C induces debromination, leading to the formation of 1D polymers (**2**). A subsequent annealing step at 420 °C promotes the cyclodehydrogenation and the consequent formation of nonbenzenoid CLPs (**3**). Interestingly, two types of C–C coupling motifs, comprising the formation of a hexagon (**3a**) or a pentagon (**3b**) between cyclopenta[*hi*]aceanthrylene subunits, are observed. Such C–C couplings arises from the presence of *s-trans* and *s-cis* isomers at the polymer step, though the formation of a hexagon, which implies cyclodehydrogenation between adjacent *s-trans*/*s-cis* and *s-cis*/*s-trans* isomers, is favoured over the formation of the pentagon (cyclodehydrogenation between adjacent *s-trans*/*s-trans* and *s-cis*/*s-cis* isomers). We expect that the synthetic strategy presented in this work is of general relevance for the synthesis of novel conjugated ladder-type polymers, and will contribute to expand the knowledge in this field with notable potential for device applications.

Conflicts of interest

There are no conflicts to declare.

Acknowledgements

This work was supported by the Swiss National Science Foundation (200020_182015), the European Union's Horizon 2020 research and innovation programme (GrapheneCore2 785219), the Office of Naval Research (N00014-18-1-2708), and the Swiss National Centre for Computational Design and Discovery of Novel Materials (MARVEL). The Swiss National Supercomputing Centre (CSCS) under project ID s904 is acknowledged for computational resources. M.K. gratefully acknowledges the generous funding by the Deutsche Forschungsgemeinschaft (DFG) – Project number 182849149 – SFB 953 "Synthetic Carbon Allotropes".

Notes and references

1 W. Metanomski, R. Bareiss, J. Kahovec, K. Loening, L. Shi and V. Shibaev, *Pure Appl. Chem.*, 1993, **65**, 1561–1580.
2 A.-D. Schlüter, *Adv. Mater.*, 1991, **3**, 282–291.
3 L. Yu, M. Chen and L. R. Dalton, *Chem. Mater.*, 1990, **2**, 649–659.
4 A. C. Grimsdale and K. Müllen, *Macromol. Rapid Commun.*, 2007, **28**, 1676–1702.
5 P. Bornoz, M. S. Prévot, X. Yu, N. Guijarro and K. Sivula, *J. Am. Chem. Soc.*, 2015, **137**, 15338–15341.
6 W. Huang, H. Zhang, J. Ma, M. Chen, H. Zhu and W. Wang, *J. Mater. Chem. C*, 2015, **3**, 6200–6208.
7 S. Che, J. Pang, A. J. Kalin, C. Wang, X. Ji, J. Lee, D. Cole, J.-L. Li, X. Tu, Q. Zhang, H.-C. Zhou and L. Fang, *ACS Mater. Lett.*, 2020, **2**, 49–54.
8 J. Chen, K. Yang, X. Zhou and X. Guo, *Chem.–Asian J.*, 2018, **13**, 2587–2600.
9 F. Trilling, M.-K. Ausländer and U. Scherf, *Macromolecules*, 2019, **52**, 3115–3122.
10 J. Lee, A. J. Kalin, C. Wang, J. T. Early, M. Al-Hashimi and L. Fang, *Polym. Chem.*, 2018, **9**, 1603–1609.
11 M. M. Durban, P. D. Kazarinoff, Y. Segawa and C. K. Luscombe, *Macromolecules*, 2011, **44**, 4721–4728.
12 M. D. Watson, A. Fechtenkötter and K. Müllen, *Chem. Rev.*, 2001, **101**, 1267–1300.
13 M. A. Abdulhamid, H. W. H. Lai, Y. Wang, Z. Jin, Y. C. Teo, X. Ma, I. Pinnau and Y. Xia, *Chem. Mater.*, 2019, **31**, 1767–1774.
14 T. Corrado and R. Guo, *Mol. Syst. Des. Eng.*, 2020, **5**, 22–48.
15 M. Morales-Vidal, P. G. Boj, J. M. Villalvilla, J. A. Quintana, Q. Yan, N.-T. Lin, X. Zhu, N. Ruangsupapichat, J. Casado, H. Tsuji, E. Nakamura and M. A. Díaz-García, *Nat. Commun.*, 2015, **6**, 8458.
16 J. Lee, A. J. Kalin, T. Yuan, M. Al-Hashimi and L. Fang, *Chem. Sci.*, 2017, **8**, 2503–2521.
17 Y. C. Teo, H. W. H. Lai and Y. Xia, *Chem.–Eur. J.*, 2017, **23**, 14101–14112.
18 B. de la Torre, A. Matěj, A. Sánchez-Grande, B. Cirera, B. Mallada, E. Rodríguez-Sánchez, J. Santos, J. I. Mendieta-Moreno, S. Edalatmanesh, K. Lauwaet, M. Otyepka, M. Medveď, Á. Buendía, R. Miranda, N. Martín, P. Jelínek and D. Écija, *Nat. Commun.*, 2020, **11**, 4567.
19 K. Biswas, J. I. Urgel, A. Sánchez-Grande, S. Edalatmanesh, J. Santos, B. Cirera, P. Mutombo, K. Lauwaet, R. Miranda, P. Jelínek, N. Martín and D. Écija, *Chem. Commun.*, 2020, **56**, 15309–15312.
20 M. Di Giovannantonio, Q. Chen, J. I. Urgel, P. Ruffieux, C. A. Pignedoli, K. Müllen, A. Narita and R. Fasel, *J. Am. Chem. Soc.*, 2020, **142**, 12925–12929.
21 Q. Shen, H.-Y. Gao and H. Fuchs, *Nano Today*, 2017, **13**, 77–96.
22 J. Cai, P. Ruffieux, R. Jaafar, M. Bieri, T. Braun, S. Blankenburg, M. Muoth, A. P. Seitsonen, M. Saleh, X. Feng, K. Müllen and R. Fasel, *Nature*, 2010, **466**, 470–473.
23 K. Kawasumi, Q. Zhang, Y. Segawa, L. T. Scott and K. Itami, *Nat. Chem.*, 2013, **5**, 739–744.
24 S. Mishra, M. Krzeszewski, C. A. Pignedoli, P. Ruffieux, R. Fasel and D. T. Gryko, *Nat. Commun.*, 2018, **9**, 1714.
25 H. Terrones, M. Terrones, E. Hernández, N. Grobert, J.-C. Charlier and P. M. Ajayan, *Phys. Rev. Lett.*, 2000, **84**, 1716–1719.

© 2021 The Author(s). Published by the Royal Society of Chemistry

Open Access Article. Published on 02 July 2021. Downloaded on 2/7/2026 7:14:46 PM.
This article is licensed under a Creative Commons Attribution-NonCommercial 3.0 Unported Licence.

26 J. Lahiri, Y. Lin, P. Bozkurt, I. I. Oleynik and M. Batzill, *Nat. Nanotechnol.*, 2010, **5**, 326–329.
27 S. Bravo, J. Correa, L. Chico and M. Pacheco, *Sci. Rep.*, 2018, **8**, 11070.
28 H. Xin and X. Gao, *ChemPlusChem*, 2017, **82**, 945–956.
29 R. Grantab, V. B. Shenoy and R. S. Ruoff, *Science*, 2010, **330**, 946–948.
30 Y. Wei, J. Wu, H. Yin, X. Shi, R. Yang and M. Dresselhaus, *Nat. Mater.*, 2012, **11**, 759–763.
31 N. M. R. Peres, F. Guinea and A. H. Castro Neto, *Phys. Rev. B: Condens. Matter Mater. Phys.*, 2006, **73**, 125411.
32 M. Di Giovannantonio, J. I. Urgel, U. Beser, A. V. Yakutovich, J. Wilhelm, C. A. Pignedoli, P. Ruffieux, A. Narita, K. Müllen and R. Fasel, *J. Am. Chem. Soc.*, 2018, **140**, 3532–3536.
33 M. Di Giovannantonio, K. Eimre, A. V. Yakutovich, Q. Chen, S. Mishra, J. I. Urgel, C. A. Pignedoli, P. Ruffieux, K. Müllen, A. Narita and R. Fasel, *J. Am. Chem. Soc.*, 2019, **141**, 12346–12354.
34 J. I. Urgel, M. D. Giovannantonio, K. Eimre, T. G. Lohr, J. Liu, S. Mishra, Q. Sun, A. Kinikar, R. Widmer, S. Stolz, M. Bommert, R. Berger, P. Ruffieux, C. A. Pignedoli, K. Müllen, X. Feng and R. Fasel, *Angew. Chem.*, 2020, **132**, 13383–13389.
35 J. I. Urgel, M. Di Giovannantonio, G. Gandus, Q. Chen, X. Liu, H. Hayashi, P. Ruffieux, S. Decurtins, A. Narita, D. Passerone, H. Yamada, S. Liu, K. Müllen, C. A. Pignedoli and R. Fasel, *ChemPhysChem*, 2019, **20**, 2360–2366.
36 L. Lafferentz, F. Ample, H. Yu, S. Hecht, C. Joachim and L. Grill, *Science*, 2009, **323**, 1193–1197.
37 C. Sánchez-Sánchez, T. Dienel, A. Nicolaï, N. Kharche, L. Liang, C. Daniels, V. Meunier, J. Liu, X. Feng, K. Müllen, J. R. Sánchez-Valencia, O. Gröning, P. Ruffieux and R. Fasel, *Chem.–Eur. J.*, 2019, **25**, 12074–12082.
38 I. C.-Y. Hou, Q. Sun, K. Eimre, M. Di Giovannantonio, J. I. Urgel, P. Ruffieux, A. Narita, R. Fasel and K. Müllen, *J. Am. Chem. Soc.*, 2020, **142**, 10291–10296.
39 J. D. Wood, J. L. Jellison, A. D. Finke, L. Wang and K. N. Plunkett, *J. Am. Chem. Soc.*, 2012, **134**, 15783–15789.
40 S. R. Bheemireddy, M. P. Hautzinger, T. Li, B. Lee and K. N. Plunkett, *J. Am. Chem. Soc.*, 2017, **139**, 5801–5807.
41 C. Weiss, C. Wagner, C. Kleimann, M. Rohlfing, F. S. Tautz and R. Temirov, *Phys. Rev. Lett.*, 2010, **105**, 086103.
42 G. Kichin, C. Weiss, C. Wagner, F. S. Tautz and R. Temirov, *J. Am. Chem. Soc.*, 2011, **133**, 16847–16851.
43 Q. Sun, O. Gröning, J. Overbeck, O. Braun, M. L. Perrin, G. Borin Barin, M. El Abbassi, K. Eimre, E. Ditler, C. Daniels, V. Meunier, C. A. Pignedoli, M. Calame, R. Fasel and P. Ruffieux, *Adv. Mater.*, 2020, 1906054.
44 M. Ammon, T. Sander and S. Maier, *J. Am. Chem. Soc.*, 2017, **139**, 12976–12984.

© 2021 The Author(s). Published by the Royal Society of Chemistry